Organic Electronics 25 (2015) 245–253

Contents lists available at ScienceDirect

Organic Electronics

journal homepage: www.elsevier.com/locate/orgel

Investigation of benzo(1,2-b:4,5-b′)dithiophene as a spacer in organic dyes for high efficient dye-sensitized solar cell

Xiaole Zhou [a,1], Xianghong Li [b,1], Yuwen Liu [a], Renjie Li [a,*], Kejian Jiang [c,*], Jiangbin Xia [a,*]

[a] College of Chemistry and Molecular Science, Wuhan University, Wuhan 430072, China
[b] Key Laboratory of Catalysis and Materials Science of the State Ethnic Affairs Commission & Ministry of Education, South-Central University for Nationalities, Wuhan 430074, China
[c] Laboratory of New Materials, Institute of Chemistry, Chinese Academy of Sciences, Beijing 100080, China

ARTICLE INFO

Article history:
Received 22 June 2015
Accepted 22 June 2015

Keywords:
Dye-sensitization
Organic dye
Benzo(1,2-b:4,5-b′)dithiophene

ABSTRACT

Two benzo(1,2-b:4,5-b′)dithiophene (denoted as BDT) based organic dyes, Dye 1 and Dye 2, containing triphenylamine and carbazole in the molecular frameworks respectively, were synthesized, characterized and applied in dye-sensitized solar cells (DSSCs). The photo-physical, photovoltaic, and electrochemical properties of the two dyes were analyzed in this work. The two dyes exhibit strong charge transfer absorption bands in the visible region. The dyes were applied in dye sensitized solar cells obtaining 11.34 mA/cm^2, 0.75 V and 0.74, for the short-circuit photocurrent density (J_{sc}), open-circuit voltage (V_{oc}), and fill factor (FF) respectively, corresponding to an overall power conversion efficiency of 6.3%. These results revealed that BDT-based dyes are promising dyes for DSSCs.

1. Introduction

Dye-sensitized solar cell (DSSC) technology has attracted much interest not only at academic level but also at industry level since is the 3rd-generation solar cell technology closest to commercialization [1–3]. DSSC devices comprise a transparent conducting oxide made of fluorine doped tin oxide (FTO) on glass, a nanoporous TiO_2 film electrode which is sensitized with a dye, an electrolyte and a back metal Pt counter electrode. Among these components, the dye is one of the most important component since it can be engineered to increase the power conversion efficiency of the solar cell [3–6]. Research on novel dyes is nowadays focused on obtaining high molar absorption coefficients, so the dye can adsorb in the visible and near-infrared wavelengths and exhibit enhanced light harvesting capacity [6–26]. Organic dyes are very attractive molecules due to their lower cost, ease for structure tunability and high molar extinction coefficients [15–26] if compared to Ruthenium-based sensitizers [3–13]. New dyes with the donor-π-acceptor concept has been widely recognized in DSSCs for enhancing light harvesting capacity [15–26]. This concept initiated with the polymer heterojunction solar cells, and a successful example is the breakthrough observed with the application of the novel low band gap polymer containing the benzo[1,2-b:4,5-b′]dithiophene moiety (BDT) [27–30]. The BDT has been recognized to favor light harvesting, thermal stability and high open-circuit voltage in polymer heterojunction solar cells [27–30] and in this work we want to explore the possibility to design new organic dyes based on the BDT unit concept and to obtain more stable and rigid π-conjugated condensed-polycyclic structures. Different from the recently-reported BDT derivatives [22–24], we introduced not only triphenylamine but also carbazole building blocks with the BDT unit. We use ethylene linkage instead of the bulk thiophene rings. Moreover, two long alkyl chains were further grafted on BDT to suppress the aggregation of organic dyes [23] (see Scheme 1). Herein, the two dyes were synthesized and characterized carefully. The photo-physical and photo-electric properties of these two dyes were systemically observed to get useful information for the discovery of new dyes. Notably, the two new organic dyes with triphenylamine and carbazole indeed have extended absorption edge with maximum absorption band at 520 nm and 504 nm in dichloromethane solutions and high molar absorption coefficients over 25×10^3 M^{-1} cm^{-1}, respectively. Especially, the Dye 1-based DSSCs showed a high conversion efficiency of up to 6.3% without chenodeoxycholic acid (CDCA) as an anti-aggregation agent, while reference ruthenium dye of N719 gives 8.8% of efficiency under the same conditions.

* Corresponding authors at: Wuhan University, Department of Chemistry, China.
E-mail addresses: rjli@whu.edu (R. Li), kjjiang@iccas.ac.cn (K. Jiang), jbxia@whu.edu.cn (J. Xia).
[1] These authors made an equal contribution.

http://dx.doi.org/10.1016/j.orgel.2015.06.033
1566-1199/

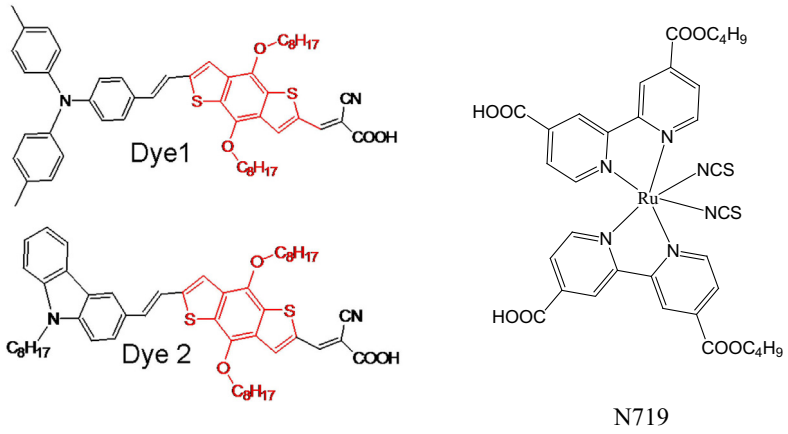

Scheme 1. Chemical structures of Dye 1, Dye 2 and N719.

2. Experimental details

2.1. Materials and reagents

All the solvents and reagents, unless specify, were of analytical grade and used as received without further purification. Tetrahydrofuran (THF) and 1,2-dichloroethane (DCE) were dried over CaH_2 and freshly distilled prior to use. The dimethyl fumarate (DMF) was dried over CaH_2 and freshly distilled under reduced pressure.

2.2. Analytical instruments

The ^1H NMR and ^{13}C NMR spectra were recorded on a Bruker (AV 300 MHz or 400 MHz) spectrometer in $CDCl_3$ and DMSO-d_6 as solvents. The chemical shifts are reported in the d-scale downfield from the peak for tetramethylsilicane. Absorption spectra were recorded on a UV-2550 spectrophotometer. Emission spectra were obtained on a LS 55 fluorescence spectrophotometer. The elemental analyses were determined by Vario EL III O-Element Analyzer system. Mass spectra were recorded on a VG70-250S mass spectrometer. The redox potentials were measured by using cyclic voltammetry on a CHI 620 analyzer. All measurements were carried out in CH_2Cl_2 solutions containing 0.1 M tetrabutylammonium hexafluorophosphate ($TBAPF_6$) as the supporting electrolyte under ambient conditions after purging with N_2 for 10 min. The conventional three electrode configuration was employed, which consists of a glassy carbon working electrode, a platinum counter electrode, and a Ag/Ag^+ reference electrode calibrated with ferrocene/ferrocenium (Fc/Fc^+) as an internal reference.

2.3. Computational details

The hybrid density functional Becke–Lee–Young–Parr composite of exchange–correlation functional method was used for both geometry optimizations and property calculations [31,32]. In all cases, the 6-31G (d) basis set was used. Berny algorithm using redundant internal coordinates was employed in energy minimization and the default cutoffs were used throughout. Using the energy-minimized structures generated in the previous step, normal coordinate analyses were carried out.

2.4. General procedure for fabrication and characterization of DSSCs

The nanocrystalline TiO_2 pastes (particle size, 20 nm) were prepared using a previously reported procedure [3]. Herein, fluorine doped thin oxide (FTO, 4 mm thickness, 10 $\Omega\,sq^{-1}$, Nippon Sheet Glass, Japan) conducting electrodes were washed with soap and water, followed by sonication for 10 min in acetone and isopropanol, respectively. After drying, the electrodes were submerged in a 40 mM aqueous solution of $TiCl_4$ for 30 min at 75 °C, and then washed with water and ethanol, respectively. An 11 μm thick nanocrystalline TiO_2 layer and a 6 μm thick TiO_2 light scattering layer (particle size, 400 nm, PST-400C) were coated on the electrodes by the screen-printing method. The double-layer TiO_2-coated electrodes were heated at 500 °C for 30 min, then treated with a 40 mM of $TiCl_4$ solution for 30 min at 75 °C and subsequent sintered at 500 °C for 30 min again. After cooling, the electrodes were soaked in a 4-tert-butanol–acetonitrile–tetrahydrofuran (1:1:0.2, v/v) solution with 0.2 mM dyes and 2 mM 3a,7a-dihydroxy-5b-cholic acid (chenodeoxycholic acid), which were kept at room temperature under dark for 24 h. Herein, the thickness of TiO_2 films was measured using a profiler, Sloan, Dektak3.

The dye-adsorbed TiO_2 electrode washed with ethanol and dried. A platinum-coated counter electrode was prepared according to a previous report [3], and two holes were drilled on its opposite sides. The two electrodes were sealed together with a 25 mm thick thermoplastic Surlyn frame. After that a drop of electrolyte solution was then introduced through one of the two holes in the counter electrode, and the holes were sealed with the thermoplastic Surlyn. The electrolyte consisted of 0.68 M dimethyl imidazolium iodide, 0.05 M iodine, 0.10 M LiI, 0.05 M guanidinium thiocyanate, and 0.40 M tertbutylpyridine in the mixture of acetonitrile and valeronitrile (85:15, v/v). All the devices were prepared with a photoactive area of about 0.3 cm^2, and a metal mask of 0.165 cm^2 was used to cover the device for photovoltaic property measurements.

2.5. The detailed experimental procedures and characterization data

Thiophene-3-carbonyl chloride (**1**) [28], N,N-diethylthiophen e-3-carboxamide (**2**), and benzo[1,2-b:4,5-b′]dithiophene-4, 8-dione (**3**), were synthesized according to the methods reported in the literature [28] and characterized by ^1H NMR. The synthetic routes of these dyes were shown in Scheme 2, and the detailed synthetic procedures are as follows.

2.5.1. 4,8-Bis(octyloxy)benzo[1,2-b:4,5-b']dithiophene (**4**)

Compound **3** (660.8 mg, 3.0 mmol), zinc powder (579.4 mg, 9.0 mmol), together with 9 mL of water and 5 mL of THF were put into a 100 mL flask. Then 1.8 g of NaOH was added in it. The mixture was well stirred and heated to reflux for 1 h. After that, 1-bromo-octane (1.74 g, 9.0 mmol) and a catalytic amount of

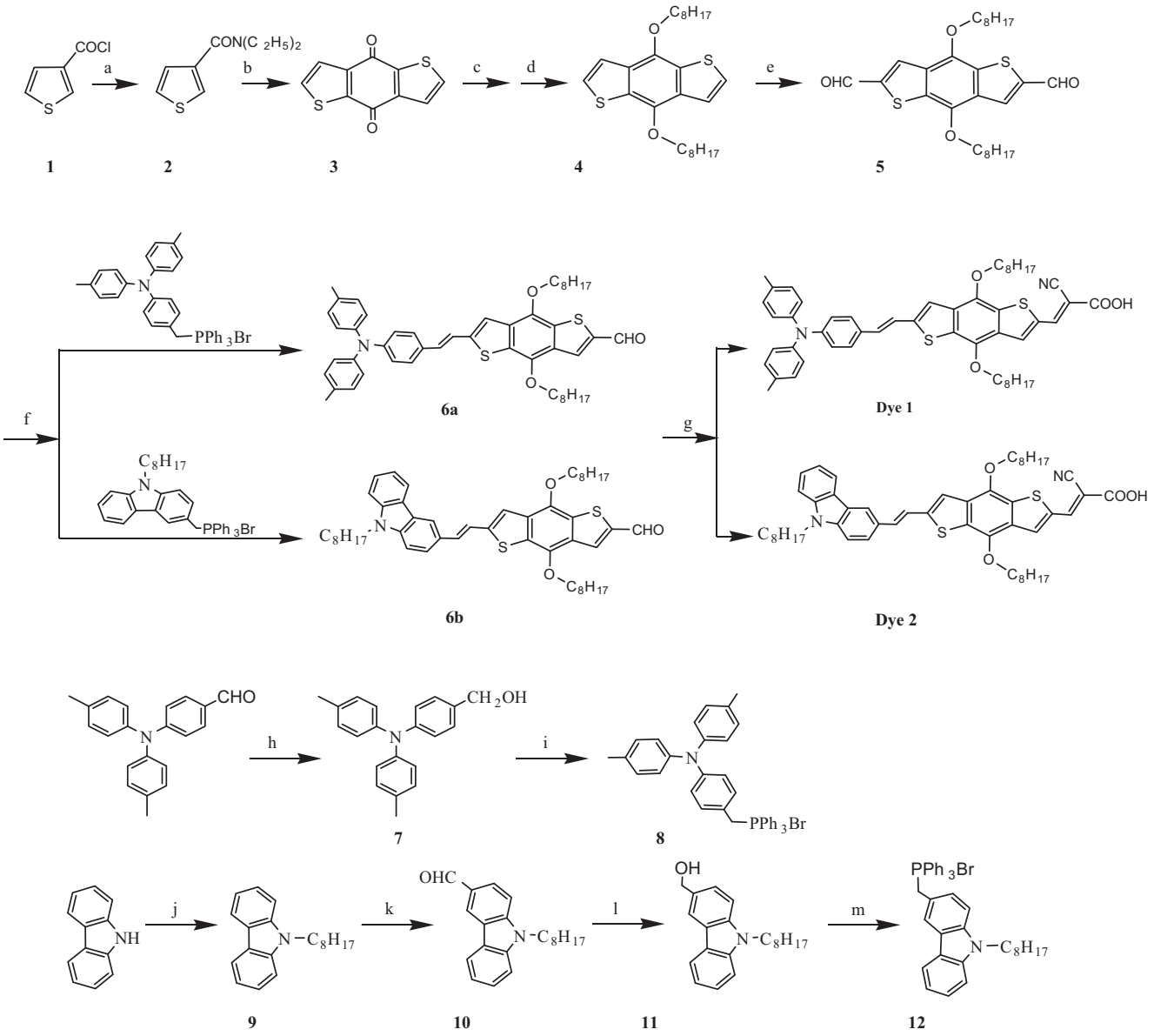

Scheme 2. The synthetic route of the dyes. The reaction conditions: (a) $HN(C_2H_5)_2$, ice water; (b) n-BuLi, ice water, N_2; (c) H_2O/Zn/NaOH, reflux for 1 h; (d) n-$C_8H_{17}Br$, (n-Bu)$_4$NBr, reflux for 2 h; (e) n-BuLi, DMF; (f) K_2CO_3, 18-crown-6; (g) $CNCH_2COOH$, piperidine; (h) $NaBH_4$, EtOH; (i) PPh_3·HBr, CH_2Cl_2; (j) $C_8H_{17}Br$, (n-Bu)$_4$NBr; (k) $POCl_3$, DMF; (l) $NaBH_4$, EtOH; (m) PPh_3·HBr, CH_2Cl_2.

tetrabutylammonium bromide were added. When the solution was turned yellow to deep red after refluxing for 2 h, an excess amount of Zn powder was added in it. The mixture was poured into cold water and extracted by 20 mL of dichloromethane for 3 times after refluxing for 6 h. The organic layer was dried over anhydrous Na_2SO_4. After removing solvent, the resulting solid was purified by column chromatography on silica gel using petroleum-dichloromethane (5:1, v/v) as eluent to give a white crystal (1.13 g, yield: 84.3%). ^{1}H NMR ($CDCl_3$, 300 MHz), δ (ppm): 7.46 (d, 2H), 7.36 (d, 2H), 4.30 (t, 4H), 1.88 (m, 4H), 1.57 (m, 4H), 1.38–1.26 (m, 16H), 0.90 (t, 6H). Anal. Calc. for $C_{26}H_{38}O_2S_2$: C, 69.64%; H, 7.95%. Found: C, 69.91%; H, 8.57%.

2.5.2. 4,8-Bis(octyloxy)benzo-dithiophene-2,6-dicarbaldehyde (**5**)

Compound **4** (495.7 mg, 1.1 mmol) was dissolved in 15 mL of anhydrous THF at ambient temperature under N_2 atmosphere. After cooling to −78 °C, 2.8 mL of n-butyllithium (6.72 mmol, 2.4 M) was added dropwise to the solution. The mixture was stirred for 3 h and 2 mL of anhydrous DMF was then added. Before pouring the reactant into 40 mL ice water, the solution was stirred for another 2 h. After the mixture stirred for 1 h, the ice water was extracted by CH_2Cl_2 for 3 times. The organic layer was dried over anhydrous Na_2SO_4 and then the solvent was removed. The resulting crude product was purified by column chromatography on silica gel using petroleum-dichloromethane (1:2,v/v) as eluent to give orange solid (366.6 mg, yield: 65.7%). ^{1}H NMR ($CDCl_3$, 300 MHz), δ (ppm): 10.15 (s, 2H), 8.20 (s, 2H), 4.37 (t, 4H), 1.91 (m, 4H), 1.57 (m, 4H), 1.36–1.29 (m, 16H), 0.89 (t, 6H). ^{13}C NMR ($CDCl_3$, 300 MHz), δ (ppm): 183.89, 146.31, 143.67, 133.01, 130.50, 130.47, 73.97, 31.24, 29.88, 28.77, 28.67, 25.38, 22.08, 13.52. Anal. Calcd for $C_{28}H_{38}O_4S_2$: C, 66.89%; H, 7.62%. Found: C, 69.92%; H, 7.87%. MS (MALDI-TOF): m/z 502.968 ($M+H^+$).

2.5.3. (4-(Di-p-tolylamino)phenyl)methanol (**7**)

4-(Di-p-tolylamino)benzaldehyde (1.2 g, 4.0 mmol) and $NaBH_4$ (90.8 mg, 2.3 mmol) were dissolved in 20 mL dry ethanol under N_2 atmosphere. Then the mixture was maintained at 60 °C for 2.5 h. When the reaction was over, an excess of water was added

to remove the unreacted $NaBH_4$. The resulting mixture was extracted by CH_2Cl_2 and then the solvent was removed to obtain the pure product **7**. It was no further purified and dissolved in 20 mL of CH_2Cl_2 for the next step.

*2.5.4. (4-(Di-p-tolylamino)benzyl)triphenylphosphonium bromide (**8**)*

PPh_3·HBr (1.38 g, 4.0 mmol) was added into the CH_2Cl_2 solution of **7** and the mixture refluxed for 4 h. Then the solvent was removed by rotary evaporation. The product was purified by column chromatography using CH_2Cl_2 and CH_2Cl_2–CH_3OH (10:1, v/v) as eluent continuously. The compound **8** was then obtained as a solid (2.24 g, yield: 89.1%). ^{1}H NMR ($CDCl_3$, 300 MHz), δ (ppm): 7.74–7.63 (m, 15H), 7.04 (d, 4H), 6.91–6.75 (m, 6H), 6.73 (d, 2H), 5.23 (d, 2H), 2.29 (s, 6H).

*2.5.5. 9-Octyl-9H-carbazole (**9**)*

Carbazole (1.67 g, 10 mmol), 1-bromo-n-octane (2.41 g, 12.5 mmol) and tetrabutyl ammonium bromide (TBAB, 111.3 mg, 0.3 mmol) were added into a 100 mL flask. Then, 20 mL of 50% NaOH aqueous solutions and 5 mL of toluene were added into the flask. The reactants were stirred at 80 °C for 30 min. After cooling to room temperature, the product was extracted by CH_2Cl_2 for 3 times and yellow solid was obtained by removing the solvent. Herein, compound **9** was finally obtained as a white crystal (1.468 g, 52%) by recrystallized in ethanol and used directly in next step.

*2.5.6. 9-Octyl-9H-carbazole-3-carbaldehyde (**10**)*

$POCl_3$ (1.55 g, 9.86 mmol) was slowly added into dry DMF (1.98 g, 27.0 mmol) under N_2 atmosphere at 0 °C. Then the mixture was allowed to warm at room temperature for 1 h. The dry 1,2-dichloroethane (10 mL) solution of **9** was added dropwise into the above-mentioned solution at 0 °C. After keeping at 0 °C for 1 h, the reactants were heated at 90 °C and stirred for 8 h. When the reaction was over, the product was poured into cold water, and the pH of the aqueous solution should be adjusted to 9–10. Then, crude yellow oil was obtained by extracting with CH_2Cl_2. After purified it by column chromatography using petroleum ether: CH_2Cl_2 (3:2, v/v) as eluent, compound **10** was obtained as a light yellow oil (1.1 g, yield: 73.3%). ^{1}H NMR ($CDCl_3$, 300 MHz), δ (ppm): 10.10 (s, 1H), 8.62 (s, 1H), 8.16 (d, 1H), 8.00 (d,1H), 7.57–7.30 (m, 4H), 4.34 (t, 2H), 1.87 (t, 2H), 1.35–1.24 (m, 10H), 0.86 (t, 3H).

*2.5.7. ((9-Octyl-9H-carbazol-3-yl)methyl)triphenylphosphonium bromide (**12**)*

Herein, compound **11** was obtained as crude product by the reduction reaction of **10** and $NaBH_4$. Then it was used without further purification to synthesize compound **12** according to the procedure for the synthesis of **8**. The compound **12** was obtained as a yellow solid (1.03 g, yield: 56.58%). ^{1}H NMR ($CDCl_3$, 300 MHz), δ (ppm): 7.79–7.72 (m, 10H), 7.65–7.62 (m, 6H), 7.51–7.35 (m, 4H), 7.18–7.13 (m, 2H).

*2.5.8. 6-(4-(Di-p-tolylamino)styryl)-4,8-bis(octyloxy)benzo[1,2-b:4,5-b']dithiophene-2-carbaldehyde (**6a**)*

Compound **5** (214.3 mg, 0.426 mmol), anhydrous K_2CO_3 (121.6 mg, 0.881 mmol), and 18-Crown-6 (8.5 mg, 0.032 mmol) in a three-necked flask were dried in vacuum for 30 min and followed by adding 20 mL of dry DMF. After that, the compound **8** (271.2 mg, 0.431 mmol) was dissolved in 5 mL of dry DMF and added dropwise to the above solution with stirring under N_2 atmosphere. The mixture was stirred for another 3 h at ambient temperature and then poured into ice-water (40 mL). The precipitate was filtered off and purified by silica gel column chromatography with CH_2Cl_2-petroleum ether (2:1) as eluent to yield red oil. ^{1}H NMR ($CDCl_3$, 300 MHz), δ (ppm): 10.01 (s, 1H), 8.14 (s, 1H), 7.36–7.31 (m, 3H), 7.26 (s, 1H), 7.15 (s, 1H), 7.11–6.94 (m,10H), 4.35 (t, 2H), 4.25 (t, 2H), 2.33 (s, 6H), 1.90 (m, 4H), 1.57 (m, 4H), 1.37–1.25 (m, 16H), 0.89 (t, 6H). MS (MALDI-TOF): m/z 772.774 (M^+).

*2.5.9. 2-Cyano-3-(6-(4-(di-p-tolylamino)styryl)-4,8-bis(octyloxy)-benzo[1,2-b:4,5-b']dithiophen-2-yl) acrylic acid (Dye **1**)*

A 20 mL of acetonitrile solution containing compound **6a** (1.54 g, 2.0 mmol), cyanoacetic acid (171 mg, 2.12 mmol), and 0.20 mL of piperidine were charged sequentially in a three-necked flask and heated to reflux overnight under N_2 atmosphere. After cooling at room temperature, solvents were removed by rotary evaporation and the residue was absorbed on silica gel and purified by column chromatography using CH_2Cl_2–CH_3OH (10:1, v/v) as eluent to yield Dye 1 as a dark solid (153.6 mg, yield: 46.2%). ^{1}H NMR ($CDCl_3$, 300 MHz), δ (ppm): 8.44 (s, 1H), 8.07 (s, 1H), 7.31 (m,2H), 7.12–6.91 (m, 13H), 4.33 (t, 2H), 4.24 (t, 2H), 2.33 (s, 6H), 1.90 (m, 4H), 1.56 (m, 4H), 1.37–1.25 (m, 16H), 0.89 (t, 6H); ^{13}CNMR ($CDCl_3$, 100 MHz), δ (ppm): 189.71, 166.39, 161.13, 158.93, 145.99, 144.77, 129.99, 127.82, 127.64, 125.16, 121.58, 99.99, 98.18, 82.67, 75.26, 74.27, 60.55, 56.88, 54.29, 52.84, 52.37, 31.85, 30.49, 29.97, 29.42, 29.30, 26.03, 22.66, 20.85, 20.71, 14.10, 13.72; MS (MALDI-TOF): m/z 839.766 ($M+H^+$); Calcd. For $C_{52}H_{58}N_2S_2O_4$: C, 74.43%; H, 6.97%; N, 3.34%; Found: C, 73.96%; H, 6.79%; N, 3.59%.

*2.5.10. 6-(2-(9-Octyl-9H-carbazol-3-yl)vinyl)-4,8-bis(octyloxy)benzo-[1,2-b:4,5-b']dithioph-ene-2-carbaldehyde (**6b**)*

Product **6b** was synthesized according to the procedure of the synthesis of **6a**. The crude compound was purified by column chromatography using CH_2Cl_2–CH_3OH (10:1, v/v) as eluent to give red oil. The resulting product was pure enough to be used in the next procedure. Therefore, no further characterization was preceded.

*2.5.11. 2-Cyano-3-(6-((E)-2-(9-octyl-9H-carbazol-3-yl)vinyl)-4,8-bis(octyloxy)benzo[1,2-b:4,5-b']-dithiophen-2-yl)acrylic acid (Dye **2**)*

Product Dye **2** was synthesized and purified according to the procedure of Dye **1**, giving dark red solid. It is noted that all the peaks of Dye 2 in ^{1}HNMR spectrum were broaden and no obvious coupling splits were observed. ^{1}H NMR (d_6-DMSO, 300 MHz), δ (ppm): 8.50 (s,1H), 8.40 (s, 1H), 8.32 (s, 1H), 8.13 (s, 1H), 7.72 (s, 1H), 7.63–7.46 (m, 5H), 7.22 (m, 2H), 4.31 (m, 4H), 4.24 (s, 2H), 1.81 (m, 6H), 1.53 (s, 4H), 1.32–1.16 (m, 27H), 0.85–0.81 (m, 9H). ^{13}CNMR (d_6-DMSO, 100 MHz), δ (ppm): 211.24, 157.97, 143.27, 131.79, 128.55, 127.54, 99.99, 94.52, 88.63, 74.38, 74.09, 56.49, 42.82, 31.73, 31.72, 31.61, 30.42, 29.28, 29.23, 29.14, 29.05, 28.96, 26.91, 25.99, 25.88, 22.57, 22.56, 22.45, 19.01, 14.40, 14.38, 14.32; MS (ESI-MS negative mode): m/z 843.44 ($[M-H^+]^-$); Calcd. For $C_{52}H_{64}N_2S_2O_4$: C, 73.89%; H, 7.63%, N, 3.31%; found: C, 73.60%; H, 7.79%; N, 3.59%.

3. Results and discussion

3.1. Synthesis and characterization

The molecular structures and synthetic routes of the two organic dyes Dye **1** and Dye **2** are shown in Schemes 1 and 2, respectively. The two dyes were synthesized by the stepwise synthetic protocol. The main material, compound **5**, prepared from compound **4**, was initially obtained by the vilsmeier reaction using $POCl_3$-DMF system [20]. However, many by-products were found in the final product which made the purification difficult. Thus, we employed the BuLi-DMF system, obtaining compound **5** with a satisfied yield of 66%. We attribute this high yield to the low temperature at which the reaction took place at −78 °C.

As shown in Scheme 2, the extension of p-conjugated aryl chain in compound **5** was carried out by the Wittig reaction obtaining the 4-(di-p-tolylamino)styryl or 2-(9-octyl-9H-carbazol-3-yl)vinyl moiety (compound **6**). It is observed that compound **6** should keep one (should keep one what? substituents? "one of the two substituents") leaving the aldehyde group. Therefore, different concentration of t-BuOK and BuLi were used as base in the reaction. The compound **6** was then easily obtained and used in the next reaction [19]. Finally, the Knoevenagel condensation reactions of aldehyde derivatives **6a** and **6b** with cyano-acetic acid resulted in the obtention of Dye **1** and Dye **2** in the presence of piperidine. These two dyes were purified by column chromatography before measurements of the physical and electrochemical properties as well as solar cell devices fabrication.

3.2. Photophysical and electrochemical properties

The visible absorption spectra of the two dyes in different solvents are shown in Fig. 1. Analysis of the dyes by UV–Vis revealed a blue-shift in the maximum absorption band when the dyes were dissolved in solvents with increasing polarity. This blue-shift may be attributed to a solvatochromic effect or to the tendency of the molecules to form aggregates. It is observed that the addition of CDCA as anti-aggregate agent results in the blue-shift of the absorption peaks of dyed-TiO_2 (see Figs. S1 and S2). These results demonstrates that the two long alkyl chains can effectively suppress dye aggregation [23,33]. On the other hand, it appeared that the polar solvents can interact with the carboxylic acid unit more effectively and led to weaken the strength of the O–H bond. This may diminish the electron-accepting ability of the acceptor moiety, which in turn can cause a reduction in donor–acceptor interaction in the dyes and as a consequent the blue shift in the absorption bands is observed [34–35]. Next, the absorption bands in CH_2Cl_2 solutions were studied. In CH_2Cl_2 solution, they exhibit two distinct absorption bands: one in the low-energy region (<400 nm) corresponding to the π–π^* transitions of the conjugated molecules, and a second one in the visible region (400–650 nm), assigned to an intramolecular charge transfer (ICT) between the electron donating unit and the cyano-acrylic acid anchoring moiety through the cross-conjugated bridge. It can be seen that the maximum absorption in visible region is centered at 520 nm ($\varepsilon = 39{,}500\ M^{-1}\ cm^{-1}$) for Dye 1 and 500 nm ($\varepsilon = 27{,}100\ M^{-1}\ cm^{-1}$) for Dye **2**, respectively. As depicted in Table 1, the molar extinction coefficient (ε) of the ICT bands of Dye **1** is higher than that of Dye **2**, indicating a stronger ability of light harvesting of Dye **1**. However, they exhibited weak emission in dichloromethane solutions and strong emission in ethanol solution around 570 nm, when excited at 460 nm. As shown in Fig. 2, the maximum emission of Dye 2 (560 nm) is blue-shifted in comparison with Dye 1 (578 nm), which indicates that Dye 2 needs more energy to be photoactivated from the ground state to the excited state. These results are in well-agreement with their corresponding absorption spectra. The normalized absorption and emission spectra of Dye **1** and Dye **2** in ethanol solutions are shown in Fig. 2. The E_{0-0} (zero–zero transition energies) were estimated from the intersection points of normalized absorption and emission spectra as 2.38 and 2.50 eV for Dye **1** and Dye **2**, respectively [36,37].

The absorptions of the two dyes on TiO_2 films were also investigated. As seen in Fig. 3, the absorption spectra of the dyes on the surface of the mesoporous TiO_2 films were broadened and red-shifted in about *ca.* 18–24 nm with respect to those in CH_2Cl_2 solution (see Table 1). Another noteworthy feature in the spectra of the dyes adsorbed on TiO_2 surface, is that the addition of CDCA as co-adsorbent leads to relative narrower absorption wavelength range and much smaller adsorption amounts in both Dye 1 and Dye 2 (see Figs. S1, S2 and Table 2). These results indicate that the aggregation of the dyes is not taking place, this is

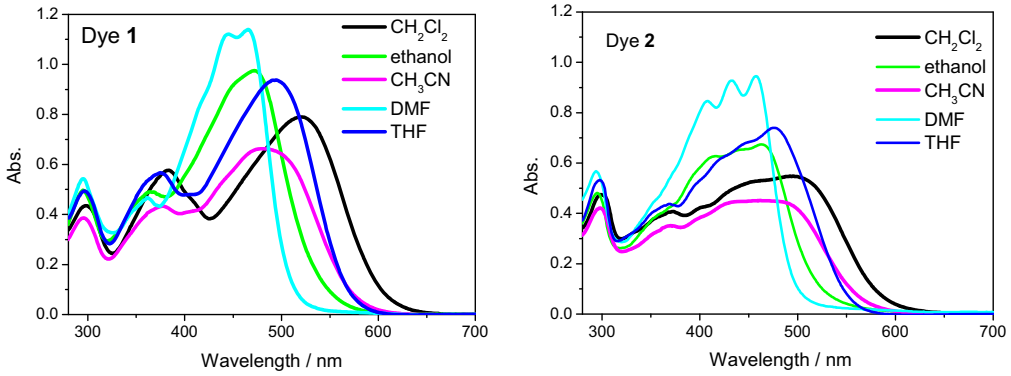

Fig. 1. The UV–Vis absorption spectra of Dye 1 and Dye 2 in different solvents ($c = 2 \times 10^{-5}$ mol dm^{-3}).

Table 1
Calculated (DFT/B3LYP) and experimental parameters of two dyes.

Dye	HOMO/LUMO[a] (eV)	Band gap[a]	λ_{abs}[b] nm, $\varepsilon/M^{-1}\ cm^{-1}$	λ_{abs}[c] nm	E_{ox}[d]	HOMO/LUMO[e] (eV)	E_{0-0}[f]	E^*[g]
Dye 1	−4.99/−2.76	2.23	520(39500)	538	0.96	−4.91/−2.53	2.38	−1.42
Dye 2	−5.23/−2.75	2.48	500(27100)	524	1.09	−5.00/−2.52	2.50	−1.41

[a] DFT/B3LPY calculated values.
[b] Absorptions measured in CH_2Cl_2.
[c] Absorptions measured on TiO_2 film.
[d] Oxidation potentials of dyes in CH_2Cl_2 containing 0.1 M Bu_4NPF_6. (Vs Ag^+/Ag) with ferrocene/ferrocenium (Fc/Fc^+) as an internal reference and converted to NHE by addition of 450 mV.
[e] HOMO and LUMO calculated by $E_{HOMO} = -(E_{ox,onset} + 4.8 - E^+_{Fc/Fc})$ eV, $E_{LUMO} = E_{HOMO} + E_{Opt}$.
[f] E_{0-0} determined from the intersection of absorption and emission in ethanol.
[g] E^* calculated by $E_{ox} - E_{0-0}$.

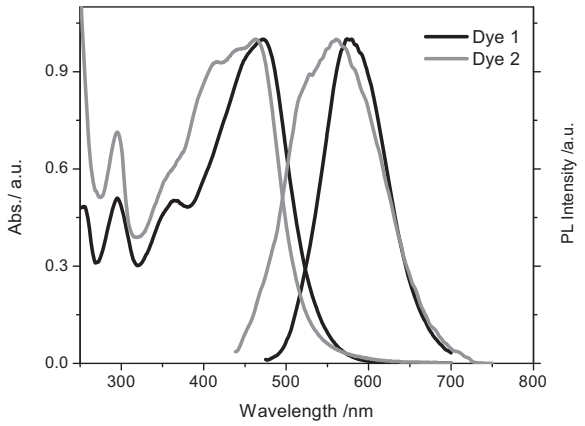

Fig. 2. Normalized electronic absorption and emission spectra of Dye **1** and Dye **2** in ethanol solutions. The emission spectra were obtained by excitation at 460 nm.

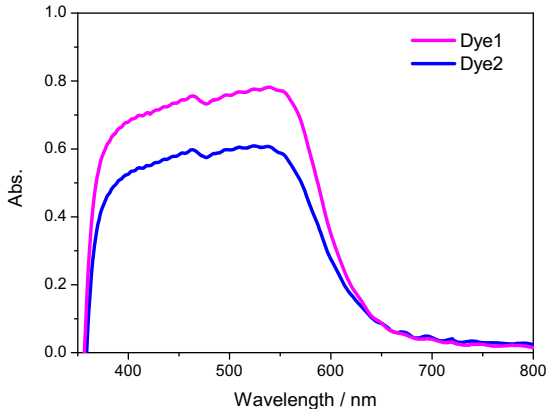

Fig. 3. The UV–Vis absorption spectra of Dye 1 and Dye 2 without CDCA absorbed on 10 μm-thick TiO_2 film.

probably due to the introduction of the bulk moieties and long alkyloxy chains on the BDT unit that inhibits the formation of the aggregates. However, the adsorption amounts of Dye 1 on TiO_2 films were much smaller than those of Dye 2, while Dye **1** exhibited higher absorption than that of Dye **2** in the range of 360–600 nm, indicating that Dye **1** has better light harvesting capability on TiO_2 films. Once again, these results are in well-agreement with the absorption spectra obtained in solution.

The electrochemical properties of Dye 1 and Dye 2 were further analyzed by cyclic voltammetry (CV) measurements, which were carried out in a 0.1 M solution of Bu_4NPF_6 in CH_2Cl_2. The reported potentials were calibrated against the ferrocene/ferrocenium (Fc/Fc^+) couple, used as the internal standard. The redox potentials and HOMO, LUMO levels [38] calculated from the oxidation potentials are summarized in Table 1. The first oxidation peaks for Dye 1 and Dye 2 are +0.96 and +1.09 V vs normal hydrogen electrode (NHE), respectively. The oxidation potentials are higher than iodine/iodide redox potential (+0.4 V vs NHE), ensuring that there is enough driving force for efficient regeneration of the dye through the recapture of the injected electrons by the dye cation radical. On the other hand, the first redox behavior was used to estimate excited-state redox potentials of the two dyes by subtracting E_{0-0} from E_{ox}. The excited-state redox potentials of Dye 1 and Dye 2 are −1.42 and −1.41 V vs NHE, which are lower than the conduction band edge of TiO_2 (−0.5 V vs NHE). This fact indicates that electrons from TiO_2 undergo no reductive reaction with ground state dyes, and carrier separation occurs fast from the exited dyes on TiO_2. This result indicates that the redox energy levels of Dye 1 and Dye 2 makes these dyes suitable as sensitizers in DSSCs.

3.3. Density functional theory (DFT)

To gain further insight into the molecular structure and frontier molecular orbitals of the two dyes, the geometries of the dyes are optimized by density functional theory (DFT) calculations at the B3LYP/6-31G(d) level. In principle, the different substitutes can modify the molecular orbital energy levels. As seen from Fig. 4, the HOMO of the asymmetrical thiophene derivatives are essentially isolated from the HOMO-1, which lie at 0.66 eV and 0.55 eV below their respective HOMO levels. The LUMO levels with the LUMO + 1 less than 1.06 eV and 1.11 eV above the individual LUMO are also isolated. Therefore, Dye 1 shows narrower HOMO–LUMO gap than that of Dye **2**, which is a benefit for harvesting light with longer wavelength. This result is consistent with the above UV–Vis absorption spectra. On the other hand, because LUMO energies of the two dyes are higher than the TiO_2 conduction band (−3.90 eV), the electron injection process is energetically favorable compared with the conduction band edge energy level of TiO_2 electrode. And their HOMO energies are lower than I^-/I_3^- potential (−4.85 eV) [33], indicating that their ground-state sensitizers regeneration are energetically favorable in DSSCs. The calculated HOMO–LUMO energies (Table 1) are fully consistent with electrochemical measurements, showing a HOMO (LUMO) onset at −4.91/−5.00 (−2.53/−2.52) eV for Dye 1 and Dye 2, respectively, in good agreement with the calculated values at −4.99/−5.23 (−2.76/−2.75) eV.

Moreover, Dye 1 and Dye 2 exhibited a similar localization of HOMO and LUMO (see Fig. 5). For Dye **1**, the HOMO is delocalized over the entire molecule except the tail of the thiophene unit. The LUMO is localized on BDT group and the acrylic acid, whereas the LUMO + 1 is localized on the BDT group with ethylene. The LUMO + 2 is localized on triphenylamine and LUMO is a π^* orbital delocalized across the thiophene frame moving to the carboxyl group. Since dyes are adsorbed onto TiO_2 films through the carboxylic acid, the presence of a LUMO on the acrylic acid indicates that the photo-excited electrons can transfer from the thiophene skeleton to the carboxyl group, which is a benefit to the injection of the photo-excited electrons to the TiO_2 CB [34]. The similar distribution observed for Dye 2 indicated that the molecule may also provide efficient electron injection into the TiO_2 CB.

Table 2
Photovolatic performances of DSSCs sensitized by Dye 1, Dye 2 and N719.

Dye	J_{sc} (mA/cm^2)	V_{oc} (V)	FF	η (%)	Adsorption amounts (mol L^{-1} cm^{-2})
Dye 1	11.34	0.75	0.74	6.30	2.67×10^{-5}
Dye 1 with CDCA	9.50	0.77	0.71	5.21	9.85×10^{-6}
Dye 2	8.21	0.67	0.76	4.18	4.36×10^{-5}
Dye 2 with CDCA	7.67	0.71	0.74	4.03	2.38×10^{-5}
N719	17.20	0.75	0.69	8.85	

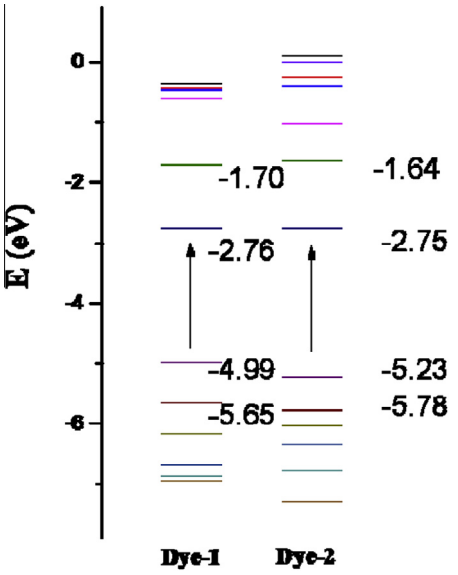

Fig. 4. Molecular orbital energy levels of the asymmetrical thiophene derivatives.

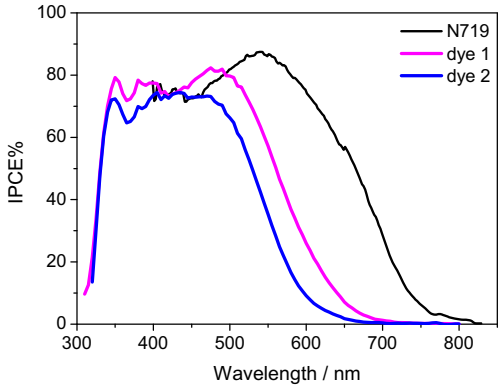

Fig. 6. Photocurrent action spectra of TiO_2 film electrodes sensitized by Dye 1, Dye 2 and N719.

3.4. DSC performance

The Fig. 6 shows the action spectra in the form of monochromatic incident photon-to-current conversion efficiency (IPCE). The Dye **1** based device clearly exhibited a stronger and broader response in the entire visible spectral region, as compared to that of the Dye **2** based device. The former showed plateaus of over 70% from 400 to 530 nm with the highest value of 82% at 483 nm, while Dye **2** presented a relatively narrow response spectrum with the highest value of 74% at 436 nm. The higher IPCE values for Dye **1** in the whole spectrum imply efficient charge transfer upon photo-excitation. The difference between IPCE spectra is in good agreement with their difference in absorption spectra as shown in Fig. 1.

The Fig. 7 shows the short circuit photocurrent density (J_{sc}), open circuit voltage (V_{oc}), fill factor (FF), and overall conversion efficiencies (η) of the two dyes-sensitized solar cells under AM 1.5 G simulated solar light at a light intensity of 100 mW cm^{-2}, and the data are summarized in Table 2. It can be seen that the Dye **1** based device gave a short circuit photocurrent density (J_{sc}) of 11.34 mA cm^{-2}, an open circuit voltage (V_{oc}) of 750 mV and fill factor (FF) of 0.74, corresponding to an overall conversion efficiency of 6.30%, while the Dye **2** based device gave a J_{sc} of 8.21 mA cm^{-2}, V_{oc} of 670 mV, FF of 0.76 and overall conversion efficiency of 4.18% under the same testing conditions. The large difference in the efficiency comes mainly from the differences in the J_{sc} between them. The higher J_{sc} for Dye **1** is consistent with its higher and broader IPCE spectrum as compared with that for Dye 2. The electron lifetime (τ) in the TiO_2 film by impedance spectra measurement is explained (see Supporting information Fig. S3). The information on electron lifetime can be extract by using the equation of $\tau_e = 1/\omega_{mid} = 1/2\pi f_{mid}$ [39,40]. It is observed that dye-1 and dye-2 exhibit the maximum f_{mid} of 1.0 Hz, 1.78 Hz, respectively. These results show that dye-1 presents the longest τ_e of 159 ms which is longer 80% than that of dye-2 with 89 ms, and may explain the larger output of V_{oc}. The comparison between Dye 1 and Dye 2 clearly reflected the importance of molecular configuration for the solar cell devices performance.

The chenodeoxycholic acid (CDCA) was used in this work for the sensitization process to suppress the aggregation of dye molecules and improve solar cell performance. The co-adsorption of dyes on the TiO_2 surface should improve both the photocurrent and the photo-voltage of DSSC cells. However, our results show that the presence of CDCA as co-adsorbent improved slightly the open circuit voltage, and that the short circuit photocurrent density was dramatically decreased. As it is well known, a co-adsorbents would influence the intermolecular interaction among dye molecules and the extent of dye adsorption on the TiO_2 surfacel. In the case of applying the CDCA co-adsorbent, lower fill factor and lower power conversion efficiencies were observed. This could be attributed to the dye aggregation which was not effectively avoided by the use of CDCA, resulting on less dye adsorbed on the TiO_2 (as shown in Table 2). On the other hand, triphenylamine and N-octylcarbazole as donor group have relative big space block to reduce the aggregation of dye molecules [41]. It can also be playing other important roles as anti-aggregation of long alkyoxyl chains grafted on BDT units [23,33].

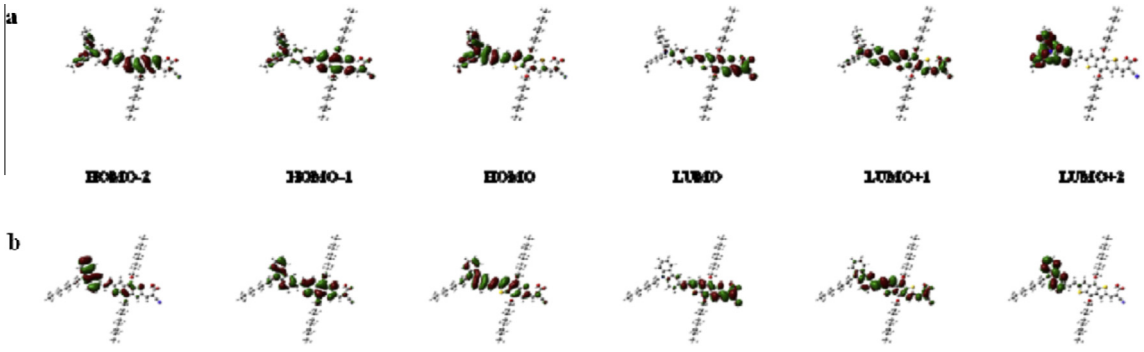

Fig. 5. Calculated molecular orbital energy levels of the asymmetrical thiophene derivatives as Dye 1 (a) and Dye 2 (b).

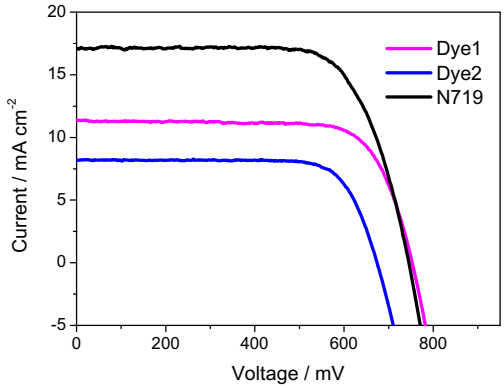

Fig. 7. The photocurrent density–voltage curve of N719, Dye 1 and Dye 2 based DSSC.

4. Conclusions

We successfully synthesized two novel organic dyes by introducing promising benzo(1,2-b:4,5-b′)dithiophene units as spacers between the donor and the acceptor. The photochemical and photoelectric properties of these two dyes were observed in detail. Dye 1 containing triphenylamine group showed relative better optic-to-electric properties based on regular liquid dye solar cell. The short-circuit photocurrent density (J_{sc}), open-circuit voltage (V_{oc}), and fill factor (FF) of the device are 11.34 mA/cm^2, 0.75 V, and 0.74, respectively, corresponding to an overall conversion efficiency of 6.3%. Comparison of these two dyes in DSSC, indicates that the large difference in power conversion efficiency comes mainly from the differences in the J_{sc}, which is directly related to the better adsorption ability of Dye **1** when adsorbed on TiO_2 films.

Acknowledgements

This work was supported by the Natural Science Foundation of China (21371138, 21301196) and the Funds for Creative Research Groups of Hubei Province (2014CFA007), the Fundamental Research Funds for the Central Universities (2042015kf0180) of China and Large-scale Instrument and Equipment Sharing Foundation of Wuhan University.

Appendix A. Supplementary data

Supplementary data associated with this article can be found, in the online version, at http://dx.doi.org/10.1016/j.orgel.2015.06.033.

References

[1] M. Grätzel, Recent advances in sensitized mesoscopic solar cells, Acc. Chem. Res. 42 (2009) 1788–1798.
[2] M.A. Green, K. Emery, Y. Hishikawa, W. Warta, Solar cell efficiency tables (Version 34), Prog. Photovoltaics Res. Appl. 17 (2009) 320–326.
[3] B. Oregan, M. Grätzel, A low-cost, high-efficiency solar cell based on dye-sensitized colloidal TiO_2 films, Nature 353 (1991) 737–739.
[4] A. Hagfeldt, M. Grätzel, Molecular photovoltaics, Acc. Chem. Res. 33 (2000) 269–277.
[5] S. Ardo, G.J. Meyer, Photodriven heterogeneous charge transfer with transition-metal compounds anchored to TiO_2 semiconductor surfaces, Chem. Soc. Rev. 38 (2009) 115–164.
[6] M.K. Nazeeruddin, P. Péchy, T. Renouard, S.M. Zakeeruddin, R. Humphry-Baker, P. Comte, P. Liska, L. Cevey, E. Costa, V. Shklover, L. Spiccia, G.B. Deacon, C.A. Bignozzi, M. Grätzel, Engineering of efficient panchromatic sensitizers for nanocrystalline TiO_2-based solar cells, J. Am. Chem. Soc. 123 (2001) 1613–1624.
[7] M. Yanagida, L.P. Singh, K. Sayama, K. Hara, R. Katoh, A. Islam, H. Sugihara, H. Arakawa, M.K. Nazeerddin, M. Grätzel, A new efficient photosensitizer for nanocrystalline solar cells: synthesis and characterization of cis-bis(4,7-dicarboxy-1,10-phenanthroline)dithiocyanato ruthenium(II), J. Chem. Soc. Dalton Trans. 16 (2000) 2817–2822.
[8] A. Islam, F.A. Chowdhury, Y. Chiba, R. Komiya, N. Fuke, N. Ikeda, L. Han, Ruthenium(II) tricarboxyterpyridyl complex with a fluorine-substituted β-Diketonato ligand for highly efficient dye-sensitized solar cells, Chem. Lett. 34 (2005) 344–345.
[9] G. Sauvé, M.E. Cass, S.J. Doig, I. Lauermann, K. Pomykal, N.S. Lewis, High quantum yield sensitization of nanocrystalline titanium dioxide photoelectrodes with cis-dicyanobis(4,4′-dicarboxy-2,2′-bipyridine)osmium(II) or Tris(4,4′-dicarboxy-2,2′-bipyridine)- osmium(II) complexes, J. Phys. Chem. B 104 (2000) 3488–3491.
[10] P. Wang, M.S. Zakeeruddin, J.E. Moser, R. Humphry-Baker, P. Comte, V. Aranyos, M.K. Nazeeruddin, M. Grätzel, Stable new sensitizer with improved light harvesting for nanocrystalline dye-sensitized solar cells, Adv. Mater. 16 (2004) 1806–1811.
[11] F. Gao, Y. Cheng, Q. Yu, S. Liu, D. Shi, Y. Li, P. Wang, Conjugation of selenophene with bipyridine for a high molar extinction coefficient sensitizer in dye-sensitized solar cells, Inorg. Chem. 48 (2009) 2664–2669.
[12] K.-M. Lee, S.-J. Wu, C.-Y. Chen, C.-G. Wu, M. Ikegami, K. Miyoshi, T. Miyasaka, K.-C. Ho, Efficient and stable plastic dye-sensitized solar cells based on a high light-harvesting ruthenium sensitizer, J. Mater. Chem. 19 (2009) 5009–5015.
[13] J.-F. Yin, M. Velayudham, D. Bhattacharya, H.-C. Lin, K.-L. Lu, Structure optimization of ruthenium photo sensitizers for efficient dye-sensitized solar cells – a goal toward a "bright" future, Coord. Chem. Rev. 256 (2012) 3008–3035.
[14] L. Yu, X. Zhou, Y. Yin, Y. Liu, R. Li, T. Peng, Highly asymmetric tribenzonaphtho-condensed porphyrazinatozinc complex: an efficient near-infrared sensitizer for dye-sensitized solar cells, ChemPlusChem 77 (2012) 1022–1027.
[15] Q.H. Yao, F.S. Meng, F.Y. Li, H. Tian, C.H. Huang, Photoelectric conversion properties of four novel carboxylated hemicyanine dyes on TiO_2 electrode, J. Mater. Chem. 13 (2003) 1048–1053.
[16] H. Tian, X. Yang, R. Chen, Y. Pan, L. Li, A. Hagfeldt, L. Sun, Phenothiazine derivatives for efficient organic dye-sensitized solar cells, Chem. Commun. (2007) 3741–3743.
[17] M. Wang, M. Xu, D. Shi, R. Li, F. Gao, G. Zhang, Z. Yi, R. Humphry-Baker, P. Wang, S.M. Zakeeruddin, M. Grätzel, High-performance liquid and solid dye-sensitized solar cells based on a novel metal-free organic sensitizer, Adv. Mater. 20 (2008) 4460–4463.
[18] N. Robertson, Catching the rainbow: light harvesting in dye-sensitized solar cell, Angew. Chem. Int. Ed. 47 (2008) 1012–1014.
[19] G. Li, K.-J. Jiang, Y.-F. Li, S.-L. Li, L.-M. Yang, Efficient structural modification of triphenylamine-based organic dyes for dye-sensitized solar cells, J. Phys. Chem. C 112 (2008) 11591–11599.
[20] K.-J. Jiang, K. Manseki, Y.-H. Yu, J.-B. Xia, L.-M. Yang, Y.-L. Song, S. Yanagida, A novel ruthenium-free TiO_2 sensitizer consisting of di-p-tolylaminophenyl ethylenedioxythiophene and cyanoacrylate groups, New J. Chem. 33 (2009) 1973–1977.
[21] Y.J. Chang, P.-T. Chou, S.-Yu. Lin, M. Watanabe, Z.-Q. Liu, J.-L. Lin, K.-Y. Chen, S.-S. Sun, C.-Y. Liu, T.J. Chow, High-performance organic materials for dye-sensitized solar cells: triarylene-linked dyads with a 4-tert-butylphenylamine donor, Chem. Asian J. 7 (2012) 572–581.
[22] X. Hao, M. Liang, X. Cheng, X. Pian, Z. Sun, S. Xue, Organic dyes incorporating the benzo[1,2-b:4,5-b′]dithiophene moiety for efficient dye-sensitized solar cells, Org. Lett. 13 (2011) 5424–5427.
[23] E. Longhi, A. Bossi, G. Di Carlo, S. Maiorana, F. De Angelis, P. Salvatori, A. Petrozza, M. Binda, V. Roiati, P.R. Mussini, C. Baldoli, E. Licandro, Metal-free benzodithiophene-containing organic dyes for dye-sensitized solar cells, Eur. J. Org. Chem. (2013) 84–94.
[24] S. Jiang, X. Lu, G. Zhou, Z.-S. Wang, Charge transfer in cross conjugated 4,8-dithienylbenzo[1,2-b:4,5-b′]dithiophene based organic sensitizers, Chem. Commun. 49 (2013) 3899–3901.
[25] J. Zhou, X. Wan, Y. Liu, Y. Zuo, Z. Li, G. He, G. Long, W. Ni, C. Li, X. Su, Y. Chen, Small molecules based on benzo[1,2-b:4,5-b′]dithiophene unit for high-performance solution-processed organic solar cells, J. Am. Chem. Soc. 134 (2012) 16345–16351.
[26] H. Tan, C. Pan, G. Wang, Y. Wu, Y. Zhang, G. Yu, M. Zhang, A comparative study on properties of two phenoxazine-based dyes for dye-sensitized solar cells, Dyes Pigm. 101 (2014) 67–73.
[27] J. Hou, M.-H. Park, S. Zhang, Y. Yao, L.-M. Chen, J.-H. Li, Y. Yang, Band gap and molecular energy level control of conjugated polymer photovoltaic Materials based on benzo[1,2-b:4,5-b′]dithiophene, Macromolecules 41 (2008) 6012–6018.
[28] Y. Liang, Y. Wu, D. Feng, S. Tsai, H. Son, G. Li, L. Yu, Development of new semiconducting polymers for high performance solar cells, J. Am. Chem. Soc. 131 (2009) 56–57.
[29] Y. Liang, Y. Wu, D. Feng, S. Tsai, G. Li, C. Ray, L. Yu, Highly efficient solar cell polymers developed via fine-tuning of structural and electronic properties, J. Am. Chem. Soc. 131 (2009) 7792–7799.
[30] L. Huo, J. Hou, Benzo[1,2-b:4,5-b′]dithiophene-based conjugated polymers: band gap and energy level control and their application in polymer solar cells, Polym. Chem. 2 (2011) (2453–246).
[31] C. Lee, W. Yang, R.G. Parr, Development of the Colle-Salvetti correlation-energy formula into a functional of the electron density, Phys. Rev. B 37 (1988) 785–789.
[32] A.D. Becke, Density-functional thermochemistry. III. The role of exact exchange, J. Chem. Phys. 98 (1993) 5648–5652.

[33] N. Koumura, Z.S. Wang, S. Mori, M. Miyashita, E. Suzuki, K. Hara, Alkyl-functionalized organic dyes for efficient molecular photovoltaics, J. Am. Chem. Soc. 128 (2006) 14256–14257.
[34] P. Singh, A. Baheti, K.R.J. Thomas, C.-H. Lee, K.-C. Ho, Fluorene-based organic dyes containing acetylene linkage for dye-sensitized solar cells, Dyes Pigm. 95 (2012) 523–533.
[35] A. Baheti, P. Tyagi, K.R.J. Thomas, Y.C. Hsu, J.T. Lin, Simple triarylamine-based dyes containing fluorine and biphenyl linkers for efficient dye-sensitized solar cells, J. Phys. Chem. C 113 (2009) 8541–8547.
[36] H. Hara, Z.S. Wang, T. Sato, A. Furube, R. Katoh, H. Sugihara, Y. Dan-oh, C. Kasada, A. Shinpo, S. Suga, Oligothiophene-containing coumarin dyes for efficient dye-sensitized solar cells, J. Phys. Chem. B 109 (2005) 15476–15482.
[37] A. Hagfeldt, M. Grätzel, Light-induced redox reactions in nanocrystalline systems, Chem. Rev. 95 (1995) 49–68.
[38] K. Kilså, E.I. Mayo, B.S. Brunschwig, H.B. Gray, N.S. Lewis, J.R. Winkler, Anchoring group and auxiliary ligand effects on the binding of ruthenium complexes to nanocrystalline TiO_2 photoelectrodes, J. Phys. Chem. B 108 (2004) 15640–15651.
[39] R. Kern, R. Sastrawan, J. Ferber, R. Stangl, J. Luther, Modeling and interpretation of electrical impedance spectra of dye solar cells operated under open-circuit conditions, Electrochim. Acta 47 (2002) 4213–4225.
[40] N. Wang, H. Lin, J.B. Li, X. Li, Improved quasi-solid dye-sensitized solar cells by composite ionic liquid electrolyte including layered α-zirconium phosphate, Appl. Phys. Lett. 89 (2006) 194104.
[41] T. Duan, K. Fan, C. Zhong, T. Peng, J. Qin, X. Chen, New organic dyes containing tert-Butyl-capped N-Arylcarbazole moiety for Dye-sensitized solar cells, RSC Adv. 2 (2012) 7081–7086.